

# Evaluation of Dynamical Properties of Open Quantum Systems Using the Driven Liouville-von Neumann Approach: Methodological Considerations

Inbal Oz,<sup>1,2</sup> Oded Hod,<sup>1,2</sup> and Abraham Nitzan<sup>1,2,3</sup>

<sup>1</sup>Department of Physical Chemistry, School of Chemistry, The Raymond and Beverly Sackler Faculty of Exact Sciences, Tel Aviv University, Tel Aviv, IL 6997801

<sup>2</sup>The Sackler Center for Computational Molecular and Materials Science, Tel Aviv University, Tel Aviv, IL 6997801

<sup>3</sup>Department of Chemistry, University of Pennsylvania, Philadelphia, PA, USA 19103

## Abstract

Methodological aspects of using the driven Liouville-von Neumann (DLvN) approach for simulating dynamical properties of molecular junctions are discussed. As a model system we consider a non-interacting resonant level uniformly coupled to a single Fermionic bath. We demonstrate how a finite system can mimic the depopulation dynamics of the dot into an infinite band bath of continuous and uniform density of states. We further show how the effects of spurious energy resolved currents, appearing due to the approximate nature of the equilibrium state obtained in DLvN calculations, can be avoided. Several ways to approach the wide band limit that is often adopted in analytical treatments, using a finite numerical model system are discussed including brute-force increase of the lead model bandwidth as well as efficient cancellation or direct subtraction of finite-bandwidth effect. These methodological considerations may be relevant also for other numerical schemes that aim to study non-equilibrium thermodynamics via simulations of open quantum systems.

## 1 Introduction

The study of electron dynamics and conductance in small electronic systems coupled to one or more free-electron reservoirs (each in its own equilibrium but not necessarily at equilibrium with

each other) has attracted much attention over the past decade due to its importance for studies in the fields of molecular electronics [1, 2, 3] spectroscopy [4], and quantum thermodynamics [5, 6, 7, 8, 9, 10, 11, 12]. Although substantial advances in observing and describing such processes were made in the past three decades, the study of particle and energy transfer in processes dominated by resonance transmission between non-equilibrium environments remains a major experimental and theoretical challenge. As in other dynamical problems, computer simulations may offer a complementary approach to purely theoretical analysis in this field.

A major challenge for modeling electronic transport through such nanometric structures is the ability to provide an appropriate non-equilibrium description of the entire (infinite in principle) system. This problem is often solved by replacing the full system by a finite system with proper account of the non-equilibrium open boundaries. One of the most widely used approaches to address this challenge is the extension of the Landauer formalism to address dynamical effects by using the non-equilibrium Green's function method [13]. This method can provide analytical solutions for non-interacting models [14, 15, 16] but it becomes computationally demanding for steady-states of more realistic model systems as well as for systems affected by time-dependent driving.

An alternative approach to describing electronic transport in such systems is the use of numerical simulations. Since simulated models are necessarily of finite size, ways to impose the infinite (in principle) nature of the real system need to be devised. In vacuum scattering problems this is usually achieved by using absorbing boundary conditions [17]. When the environment of the simulated system consists of metallic leads with occupied electronic states, the numerical boundary has to account for both electron absorption and injection. A variety of methods, too extensive to detail herein, have been developed for this purpose considering both model Hamiltonians [18, 19, 20, 21, 22, 23, 24, 25, 26, 27, 28, 29] and realistic model systems [30, 31, 16, 32, 33, 15, 34, 35, 36, 37, 38, 39, 40, 41]. Among the latter, the recently proposed Driven Liouville-von Neumann (DLvN) approach [42, 43, 44, 45], imposes the required boundary conditions by augmenting the Liouville-von Neumann (LvN) equation of motion with non-unitary source and sink terms. The latter drive each lead towards an equilibrium state determined by the chemical potential and electronic temperature of the implicit bath to which it is coupled [42, 43, 44, 45]. When the driving enforces different equilibrium states on different leads, the DLvN method was shown to provide a reliable representation of the electronic transport problem, closely reproducing the Landauer formalism results at steady-state [42, 44]. Furthermore, it was shown that, for non-interacting systems [46, 47, 48], the DLvN equation of motion can be recast into Lindblad form, thus it inherently preserves density matrix positivity [24, 44, 48]. Notably, within this approach, external dynamic perturbations such as alternating bias voltages, varying gate potentials, and time-dependent external fields may be readily imposed. These can drive the system out of its equilibrium or steady states [14] and invoke intriguing physical phenomena that are manifested in the dynamical properties of the system, beyond the scope of the well established equilibrium thermodynamic theory.

A simplistic model that can demonstrate such effects is a resonant level model, where a single non-interacting spinless state (often referred to as a quantum dot) is coupled to a manifold of non-interacting spinless lead states. Here, shifting the position of the dot level with respect to the chemical potential of the lead states mimics the application of an external time-dependent gate potential on the dot. Recent analytical analysis of this model, at the wide band limit (WBL) [49, 50, 51], enabled the calculation of thermodynamic functions to first order beyond the quasistatic (QS) limit. These were shown to fulfill the first and second laws of thermodynamics and reproduce the equilibrium and weak coupling results in the appropriate limits [5]. Such treatments, however, often rely on perturbation theory and hence are limited to cases where a small parameter can be identified. Specifically, in the treatment mentioned above, the dot level driving rate was taken to be considerably smaller than the typical internal relaxation rate of the lead. Hence, to gain access to dynamical regions that are beyond the reach of current analytical treatments of this (and more complex) model one can harness the numerical flexibility of the DLvN approach. Nevertheless, care should be taken with the practical implementation of the numerical simulation so as to ensure that the results, necessarily obtained for a finite lead model, faithfully represent the desired physical properties of an infinite environment at equilibrium. As general guidance, some rules of thumb have been introduced to assess the finite lead model size required to verify the validity of the Markovian approximation adopted in the DLvN approach [24, 48]. When numerical convergence with respect to the finite lead model size is achieved its discrete spectrum mimics well the continuous density of state of the corresponding (semi-)infinite bath. However, when using numerical simulations to extend analytical models towards new dynamical regimes, one should also keep in mind that simplifying assumptions, such as the wide band approximation (WBA), that are often invoked in approximate analytical treatments, are not always readily transferable to the numerical calculation. The present manuscript addresses these and related methodological aspects of using numerical simulations in general and, in particular, the DLvN approach to complement analytical treatments in the study of particle and heat fluxes through molecular interfaces.

## 2 Relaxation Dynamics

To set the stage for demonstrating important methodological aspects of using numerical schemes to simulate non-equilibrium scenarios, we consider first the simple relaxation dynamics of an initially occupied dot level coupled to an empty manifold of lead levels. The non-interacting Hamiltonian of the entire system is given by

$$\hat{H}(t) = \hat{H}_d(t) + \hat{H}_L + \hat{H}_V, \quad (2.1)$$

where  $\hat{H}_d(t) = \varepsilon_d(t) c_d^\dagger c_d$  is the Hamiltonian of the dot,  $\hat{H}_L = \sum_l \varepsilon_l c_l^\dagger c_l$  represents the lead section, and  $\hat{H}_V = \hat{V}_{dL} + \hat{V}_{Ld}$  is the dot/lead coupling term, where  $\hat{V}_{dL} = \sum_l (V_l d^\dagger c_l)$  and  $\hat{V}_{Ld} = \hat{V}_{dL}^\dagger$ . Here,

$\varepsilon_d(t)$  and  $\varepsilon_l$  are the energies of the dot and lead level  $l$ , respectively, and  $c_i^\dagger$  and  $c_i$  are the creation and annihilation operators for an electron in level  $i = d, l$ . Note that, for the sake of simplicity, we have assumed that the only time-dependence in the Hamiltonian stems from shifts in the position of the dot level, with no effect on the lead levels and the lead-dot coupling terms. Naturally, within the numerical treatment discussed below, this simplifying assumption can be readily lifted.

## 2.1 Analytical Solution

Under the WBA, where the manifold of lead states is assumed to be of infinite width with a uniform and continuous density of states,  $\rho$ , this model has a fully analytical solution. Upon uniformly coupling the isolated dot level to the manifold of lead states, its original delta-function shape,  $\delta(\varepsilon - \varepsilon_d)$ , broadens into a Lorentzian function of the form:

$$A(\varepsilon - \varepsilon_d; \Delta, \gamma) = \frac{1}{\pi} \frac{\hbar\gamma/2}{(\varepsilon - \varepsilon_d - \Delta)^2 + (\hbar\gamma/2)^2}. \quad (2.2)$$

Here,  $\hbar = h/(2\pi)$  is the reduced Plank's constant,  $\Delta$  represents the shift in the dot's level position due to the coupling to the lead, and  $\hbar\gamma$  is the level broadening due to its finite lifetime. The latter corresponds the leakage rate of particles from the dot to the lead manifold as given by Fermi's golden rule [52]:

$$\gamma(\varepsilon) = \frac{2\pi}{\hbar} \sum_l |V_l|^2 \delta(\varepsilon - \varepsilon_l), \quad (2.3)$$

which at the WBL, assuming an infinite lead band of constant density of states,  $\rho$ , and uniform coupling to the dot,  $V_l = V = \text{const}$ , can be evaluated as:

$$\gamma^{WBA} = \frac{2\pi}{\hbar} \int_{-\infty}^{\infty} |V_l|^2 \rho(\varepsilon_l) \delta(\varepsilon - \varepsilon_l) d\varepsilon_l = \frac{2\pi}{\hbar} |V|^2 \rho \int_{-\infty}^{\infty} \delta(\varepsilon - \varepsilon_l) d\varepsilon_l = \frac{2\pi}{\hbar} |V|^2 \rho. \quad (2.4)$$

By virtue of the Fourier transform of its Lorentzian spectral function, the population of an initially occupied dot level ( $\psi(t=0) = d^\dagger |0\rangle$ ) decays exponentially with time into the empty manifold of lead levels ( $P_d(t) = \left| \langle \psi(t=0) | e^{-\frac{i}{\hbar} \hat{H}t} | \psi(t=0) \rangle \right|^2 = e^{-\gamma t}$ ) with a characteristic decay time of  $1/\gamma$  as indicated by the dashed black line in Fig. 1.

## 2.2 Closed System Numerical Treatment

The most straightforward numerical approach to simulate this temporal behavior of the dot's population is the microcanonical scheme [16]. Here, the infinite (in principle) system is represented by a finite model consisting of the dot level uniformly coupled to a finite set of lead levels. Two important differences between this model and the one used for the analytical treatment above

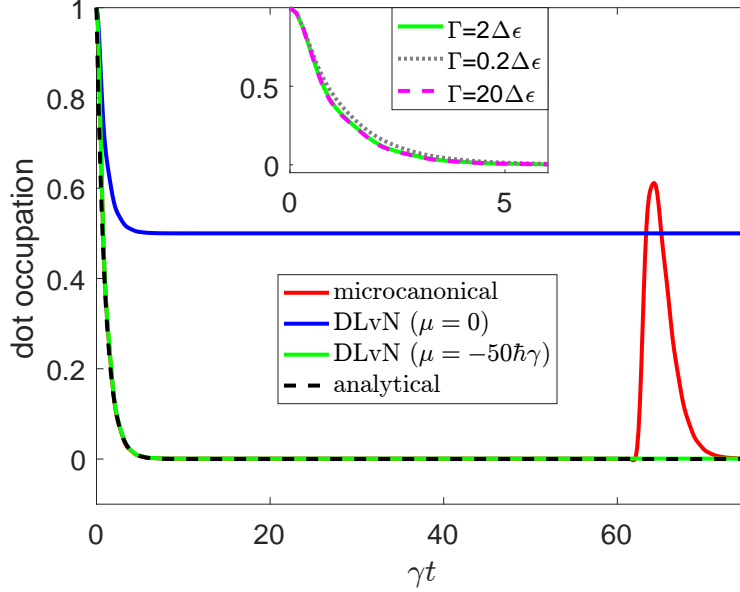


Figure 1: Dot depopulation dynamics as calculated using (i) the analytical WBA treatment (dashed black line); (ii) microcanonical simulations (full red line); (iii) DLvN simulations with an empty (green) and half filled (blue) lead. System parameters are provided in the main text. Inset: Driving rate sensitivity test of the DLvN dynamics calculated with  $\Gamma = 0.2\Delta\epsilon/\hbar$  (dashed gray),  $\Gamma = 2\Delta\epsilon/\hbar$  (green), and  $\Gamma = 20\Delta\epsilon/\hbar$  (dashed magenta).

should be noted: (i) the density of lead states is discrete, and (ii) the band of lead states is of finite width. Nevertheless, we expect that when the lead manifold is sufficiently dense and the position of the dot is far enough from the band edges, the numerical simulation will reproduce the short time dynamics of the analytical treatment. To demonstrate this, we choose a finite lead model consisting of  $N_L = 100$  equispaced levels that span a bandwidth of  $W = 10\hbar\gamma$ . The corresponding level spacing and density of states are thus given by  $\Delta\epsilon = \rho^{-1} = \frac{W}{N} = 0.1\hbar\gamma$ , respectively. The dot energy,  $\epsilon_d$ , is positioned at the center of the lead's band and is uniformly coupled to all lead levels via a coupling constant of  $V = \sqrt{\frac{\hbar\gamma}{2\pi\rho}} = \frac{\hbar\gamma}{\sqrt{20\pi}}$  (see Eq. 2.4). We note that, the choice of the specific value of  $\gamma$  (chosen herein such that  $\hbar\gamma = 0.1$  eV) is arbitrary as the results presented below are scalable with respect to it. Hence, we set all other parameters in terms of  $\gamma$  and present the result in unitless format. The dynamics of the system is simulated via the LvN equation of motion for the single-particle density matrix of the system,  $\hat{\sigma}(t)$ :

$$\frac{d}{dt}\hat{\sigma}(t) = -\frac{i}{\hbar}\left[\hat{H}(t), \hat{\sigma}(t)\right]. \quad (2.5)$$

In the basis of eigenstates of the dot and the lead sections of the system the density matrix obtains the following block representation:

$$\hat{\sigma}(t) = \begin{pmatrix} \sigma_d(t) & \hat{\sigma}_{dL}(t) \\ \hat{\sigma}_{Ld}(t) & \hat{\sigma}_L(t) \end{pmatrix}, \quad (2.6)$$

whose elements are given by  $\sigma_{ij}(t) = \langle c_i(t)c_j^\dagger(t) \rangle$ . The corresponding block matrix representation of the Hamiltonian of Eq. (2.1) is given by:

$$\hat{H}(t) = \begin{pmatrix} \varepsilon_d(t) & \hat{V}_{dL} \\ \hat{V}_{Ld} & \hat{H}_L \end{pmatrix}. \quad (2.7)$$

The initial diagonal density matrix represents a fully populated dot ( $\sigma_d(t=0) = 1$ ) and an empty lead ( $\hat{\sigma}_L(t=0) = \hat{0}$ ); In practice, we initially populate the lead levels according to a Fermi-Dirac distribution, whose chemical potential and temperature are set to  $\mu = -50\hbar\gamma$  and  $k_B T = 0.25\gamma$ , respectively). By monitoring the diagonal element of the density matrix that corresponds to the dot level we can follow its depopulation into the lead levels. The resulting dynamics, which is represented by the red curve in Fig. 1, captures well the short-time ( $\gamma t < \gamma(h\Delta\varepsilon^{-1}) = 20\pi$ , reflecting the highest frequency of the lead dynamics) exponential decay predicted by the analytical treatment. However, at longer timescales, characteristic Poincaré recurrences occur, reflecting the discrete nature of the quasi-continuum representation of the lead or, equivalently, the reflection of the scattered electron wavefunction from the far edge of the finite lead model [46, 39, 53, 54, 55, 45]. Therefore, similar to previous multi-lead microcanonical transport calculations [16, 36, 42], it becomes evident that, while microcanonical simulations are not limited to the WBA, the finite closed system model can mimic the behavior of its open counterpart only for times shorter than the typical reflection time-scale.

### 2.3 Driven Liouville-von Neumann Simulations

As mentioned above, the recently developed DLvN approach can eliminate this limitation by expanding the capabilities of the microcanonical approach to simulate truly open quantum systems. Similar to previous multi-lead implementations of the DLvN approach [42, 14, 43, 44, 46, 45, 56], the LvN equation of motion for the single-lead setup considered herein is augmented by sink and source terms that absorb outgoing electrons (thus avoiding reflections) and inject thermalized electrons near the system boundaries, respectively, as follows:

$$\frac{d}{dt}\hat{\sigma}(t) = -\frac{i}{\hbar} [\hat{H}(t), \hat{\sigma}(t)] - \Gamma \cdot \begin{pmatrix} 0 & \frac{1}{2}\hat{\sigma}_{d,L}(t) \\ \frac{1}{2}\hat{\sigma}_{Ld}(t) & \hat{\sigma}_L(t) - \hat{\sigma}_L^0 \end{pmatrix}. \quad (2.8)$$

The last term in Eq. 2.8 serves to drive the lead section towards a target equilibrium state of the form  $\sigma_{ll}^0 = \delta_{ll} f_{FD}(\varepsilon_l, \mu, T)$ , where  $f_{FD}(\varepsilon_l; \mu, T) = [\exp((\varepsilon_l - \mu)/(k_B T)) + 1]^{-1}$  is a Fermi-Dirac equilibrium distribution with the chemical potential,  $\mu$ , and electronic temperature,  $T$ , of

the electronic reservoir, to which the lead section is implicitly coupled, and  $k_B$  is Boltzmann's constant. The density matrix obtained from Eq. (2.8) is Hermitian, positive definite [44, 48], and normalized such that  $\text{tr}[\hat{\sigma}(t)] = N_{\text{tot}}(t)$ , where  $N_{\text{tot}}(t)$  is the instantaneous total number of electrons in the system.

The driving rate,  $\Gamma$ , which can be extracted from the electronic properties of the implicit reservoir [45], represents the timescale on which thermal relaxation takes place in the lead, and is generally assumed to be fast relative to all other processes of interest. If, however, the lead's driving rate is treated as a phenomenological parameter, one should make sure that the relaxation dynamics (i.e. the rate  $\gamma$ ) of the dot itself is insensitive to the choice of  $\Gamma$ . Since the latter broadens the lead levels, the  $\delta$ -functions appearing in Eq. (2.3) for the dot's relaxation rate should be replaced by the corresponding Lorentzian functions of the form  $L_l(\varepsilon - \varepsilon_l) = \frac{1}{\pi} \frac{\hbar\Gamma/2}{(\varepsilon - \varepsilon_l)^2 + (\hbar\Gamma/2)^2}$ , such that  $\gamma(\varepsilon) = 2\pi/\hbar \sum_l |V_l|^2 L_l(\varepsilon - \varepsilon_l)$ . If  $\hbar\Gamma \gg \Delta\varepsilon$  the summand is a smooth function of  $\varepsilon_l$ , which can be approximated by the following integral:

$$\gamma(\varepsilon) \approx \frac{2\pi}{\hbar} \int_{-W/2}^{W/2} |V(\varepsilon_l)|^2 \rho(\varepsilon_l) L_l(\varepsilon - \varepsilon_l) d\varepsilon_l. \quad (2.9)$$

Moreover, if  $|V(\varepsilon_l)|^2$  and  $\rho(\varepsilon_l)$  do not (or only weakly) depend on  $\varepsilon_l$  (in practice, a softer requirement that  $|V(\varepsilon_l)|^2 \rho(\varepsilon_l)$  is independent of  $\varepsilon_l$  is sufficient), they may be taken out of the integral, and if furthermore  $\hbar\Gamma \ll W$ , the limits of the remaining integral over  $L_l(\varepsilon - \varepsilon_l)$  can be safely taken to infinity yielding a value of 1 to a good approximation. Hence, the wide band result of Eq. (2.4) stating that  $\gamma \approx 2\pi/\hbar |V|^2 \rho$  is recovered and the dynamics becomes independent of  $\Gamma$ . Thus, the lead model should be chosen sufficiently large and its energy band should be made sufficiently wide to allow for the value of  $\Gamma$  to fulfill the requirement  $\Delta\varepsilon \ll \hbar\Gamma \ll W$  [24, 47, 48], which assures that the finite lead model levels are sufficiently (but not over-)broadened to mimic the continuous density-of-state within the finite bandwidth of the corresponding bulk lead. We note in passing that the above considerations are not just technical, and have been repeatedly used to explain observations of molecular relaxation processes involving isolated (on relevant timescales) large molecules [57], where a discrete molecular spectrum appears (again on relevant timescales) to act as a continuum [5, 6, 7, 8][58].

To demonstrate the performance of this approach for the case of a single-lead setup, we repeat the dot depopulation simulations of the previous section with the same model Hamiltonian using the DLvN equation of motion (2.8) with a driving rate of  $\hbar\Gamma = 2\Delta\varepsilon = 0.2\hbar\gamma$ , within the region spanned between  $\Delta\varepsilon = 0.1\hbar\gamma$  and  $W = 100\Delta\varepsilon = 10\hbar\gamma$ . The green curve in Fig. 1 presents the dot population as a function of time obtained with the same initial conditions as those used in the microcanonical simulation described above and a target equilibrium lead density matrix of  $\sigma_W^0 = \delta_W f_{FD}(\varepsilon_l, \mu = -50\hbar\gamma, T = 0.25\hbar\gamma/k_B)$ . Clearly, the DLvN dynamics is able to reproduce both the short- and the long-term analytical exponential decay of the dot population, while eliminating

the recurrences appearing in the microcanonical simulations. Thus, it is shown that the DLvN effectively couples the closed system to an external implicit bath resulting in a characteristic open quantum system dynamics. Furthermore, when setting the implicit bath's chemical potential at the center of the lead band and equal to the dot's energy (both in the initial conditions and via the target lead equilibrium density matrix,  $\sigma_W^0 = \delta_W f_{FD}(\varepsilon_l, \mu = 0, T = 0.25\hbar\gamma/k_B)$ ), the dot equilibrates to the expected half-filled state (see blue line in Fig. 1). In order to verify that our results are insensitive to the choice of driving rate we have repeated the empty lead calculations for  $\hbar\Gamma = 0.2\Delta\varepsilon$  and  $\hbar\Gamma = 20\Delta\varepsilon$ . The comparison, presented in the inset of Fig. 1, clearly demonstrate the weak dependence of the simulated dynamics on the value of  $\Gamma$ . Notably, this holds true also for the lower value chosen, which is outside the validity range discussed above. This further demonstrates that, with appropriate choice of model parameters, the DLvN approach can effectively mimic different environmental conditions and may constitute an effective numerical scheme to complement analytical treatments in parameter regimes beyond their limiting assumptions.

### 3 Equilibrium Currents

The simple single-lead model system discussed above demonstrated how the DLvN approach can capture the *total* current flowing between the dot level and the lead manifold which, according to the analytical treatment, is given by  $J(t) = -dP_d(t)/dt = \gamma e^{-\gamma t}$ . However, in many applications, especially when evaluating thermodynamics properties, it is useful to consider not only overall currents of given observables but also their resolution with respect to other observables. For example, the total current can be written in terms of its energy resolved components as  $J = \int J(\varepsilon) d\varepsilon$ , where  $J(\varepsilon)$  is the net particle flux leaving the dot at a given energy  $\varepsilon$ . The latter can be then used to evaluate thermodynamic quantities, such as the energy flux,  $J_E = \int \varepsilon J(\varepsilon) d\varepsilon$ , carried by the particles from the dot to the lead and the total heat flux that they will produce in the environment when they eventually get equilibrated in the lead,  $J_Q = \int d\varepsilon (\varepsilon - \mu) J(\varepsilon)$ .

Such energy resolved currents can be evaluated via the numerical solution of Eq. (2.8), where the temporal variation of the occupation of lead level  $l$  is given by (see Appendix A):

$$\left(\frac{d\sigma_{ll}(t)}{dt}\right) = \frac{2}{\hbar} \Im(V_{ld}\sigma_{dl}(t)) - \Gamma(\sigma_{ll}(t) - \sigma_{ll}^0). \quad (3.1)$$

We may now identify the first term on the right-hand-side of Eq. 3.1 as the incoming particle flux from the dot into lead level  $l$  and the second term as the corresponding outgoing flux into the implicit bath. Neglecting the broadening of the lead levels due to their coupling to the bath and to the dot, the former can be used to evaluate the energy resolved particle currents leaving



the dot towards the lead at energy  $\varepsilon_l$ :

$$J_{dL}(\varepsilon_l, t) = \frac{2}{\hbar} \Im(V_{ld} \sigma_{dl}(t)), \quad (3.2)$$

and the latter approximates the particle flux leaving the lead into the implicit bath at the same energy:

$$J_{LB}(\varepsilon_l, t) = \Gamma(\sigma_{ll}(t) - \sigma_{ll}^0). \quad (3.3)$$

At equilibrium, we expect the total current and all of its energy resolved components to vanish. Nevertheless, within the DLvN approach, only the lead sections are directly equilibrated with their respective implicit baths. This is essential for simulating non-equilibrium scenarios. Therefore, since equilibration is not performed in the diagonal basis of the entire finite model system and the dot section is not explicitly equilibrated, for any finite lead model equilibrium can only be reached approximately. As a result, when setting  $d\hat{\sigma}/dt = 0$  in Eq. (2.8) for the single-lead setup considered herein (this can be readily done by solving a Sylvester equation [24] as detailed in Appendix B), non-zero dot-lead coherences  $\sigma_{d,l}$  appear in the density matrix that lead to spurious non-vanishing energy resolved equilibrium currents. This, is clearly manifested by the red curve in Fig. 2 showing the equilibrium energy resolved currents obtained for a lead model consisting of 50 equispaced levels that are spanning a bandwidth of  $W = 10\hbar\gamma$ . The lead levels, which are coupled to the dot via  $V = \sqrt{\frac{\hbar}{2\pi} \frac{\gamma}{\rho}} = \frac{\hbar\gamma}{\sqrt{10\pi}}$ , are driven at a rate of  $\Gamma = 0.4\gamma$  towards an equilibrium Fermi Dirac population with chemical potential of  $\mu = 0$  and electronic temperature of  $k_B T = 0.25\hbar\gamma$ . The highest absolute current value appears at the dot position of  $\varepsilon_d = -\hbar\gamma$ . Notably, the total dot-lead current at equilibrium, obtained by summing over all its energy resolved equilibrium components,  $J_{dL} = \sum_l J^{eq}(\varepsilon_l)$ , vanishes as expected. Nevertheless, the appearance of spurious non-vanishing energy resolved equilibrium currents jeopardizes their validity for calculating non-equilibrium thermodynamic properties, such as energy and heat fluxes.

One remedy for this problem can be found by increasing the finite lead model size. At the limit of an infinite lead, its spectrum mimics well that of the entire dot+lead system and the effect of not directly equilibrating the single dot level with the implicit bath becomes negligible. This is demonstrated in Fig. 2, where doubling the number of lead levels from 50 (red) to 100 (blue), while keeping the bandwidth at  $W = 10\hbar\gamma$  (yielding  $\Delta\varepsilon = \rho^{-1} = 0.1\hbar\gamma$ ,  $V = \frac{\hbar\gamma}{\sqrt{20\pi}}$ , and  $\Gamma = 2\Delta\varepsilon/\hbar = 0.2\gamma$ ), reduces the magnitude of the energy-resolved equilibrium currents. The effects of any residual artificial currents on the calculation of non-equilibrium thermodynamic properties can be eliminated by subtracting their equilibrium contribution from the calculated dynamic properties.

Alternatively, an ‘‘extended-molecule’’ strategy can be adopted. Here, the system is divided into three (rather than two as before) sections including (see left panel of Fig. 3): (i) the dot ( $d$ ); (ii) the lead section adjacent to the dot that is directly coupled to it ( $L$ ); and (iii) a driven lead

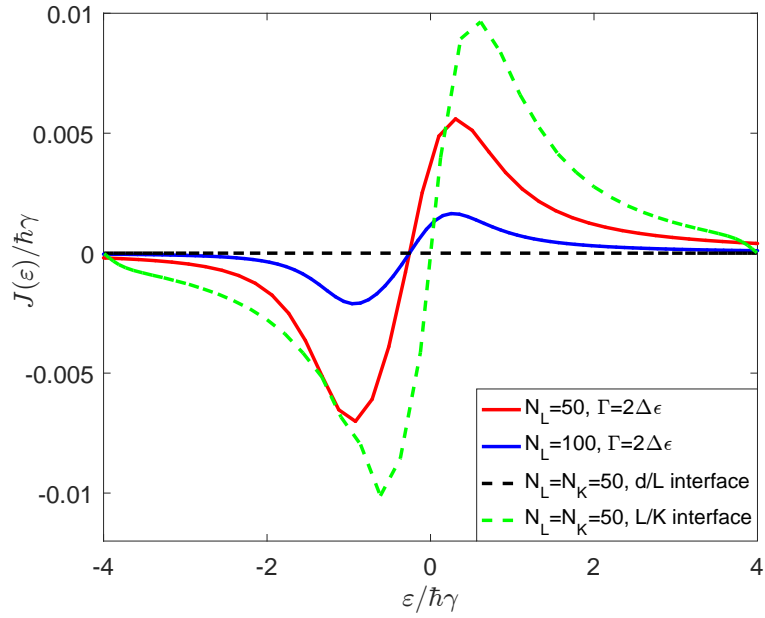


Figure 2: Spurious energy resolved equilibrium particle currents flowing between the dot and the various levels of a driven lead of  $N_L = 50$  (full red line) and  $N_L = 100$  (full blue line) levels, to which it is directly coupled. For a system composed of a dot, a lead of  $N_L = 50$  levels, and a driven-lead of  $N_K = 50$  levels the equilibrium energy resolved currents at the interface between the dot and the lead vanish (dashed black line), while those at the interface between the lead and the driven lead remain (dashed green line).

section ( $K$ ). The first two constitute the extended-dot section that is not directly coupled to the implicit bath. This buffers the dot from the effects of the open boundary conditions that are imposed only on the remote driven lead section. All physical quantities of interest can now be evaluated from the dynamics of the dot section and the dot/lead interface, where energy-resolved equilibrium currents vanish. To demonstrate this, we consider a tight-binding chain consisting of  $N_{tot} = 101$  sites, where the leftmost site serves as the dot, the  $N_L = 50$  sites adjacent to the dot form the lead section, and the remaining  $N_K = 50$  sites constitute the driven lead section. The onsite energies of the dot, the lead, and the driven lead sites are taken to be  $\alpha_d = \alpha_l = \alpha_k = 0$  eV, respectively. The hopping integrals between the various lead sites ( $\beta_l$ ), between the rightmost lead site and leftmost driven lead site ( $\beta_{lk}$ ), and between the various driven lead sites ( $\beta_k$ ), are set to  $\beta_l = \beta_{lk} = \beta_k = 0.2$  eV, respectively. A weaker coupling of  $\beta_{ld} = 0.08$  eV is chosen between the dot and the leftmost site of the lead section and all other hopping integrals are nullified. This yields a (driven-)lead bandwidth of  $W_{(driven-)lead} = 4\beta_{(k)l} = 0.8$  eV. The real-space tight-binding Hamiltonian matrix representation of the system can be written in block matrix form as follows:

$$\hat{H}(t) = \begin{pmatrix} \varepsilon_d(t) & \hat{V}_{dL} & \hat{0} \\ \hat{V}_{Ld} & \hat{H}_L & \hat{V}_{LK} \\ \hat{0} & \hat{V}_{KL} & \hat{H}_K \end{pmatrix}. \quad (3.4)$$

Here, the non-zero blocks are

$$\varepsilon_d(t) = \alpha_d; \hat{V}_{dL} = \hat{V}_{Ld}^\dagger = \begin{pmatrix} \beta_{ld} & 0 & \cdots \end{pmatrix}; \hat{H}_{L(K)} = \begin{pmatrix} \alpha_{l(k)} & \beta_{l(k)} & 0 \\ \beta_{l(k)} & \alpha_{l(k)} & \ddots \\ 0 & \ddots & \ddots \end{pmatrix};$$

$$\text{and } \hat{V}_{LK} = \hat{V}_{KL}^\dagger = \begin{pmatrix} \vdots & \vdots & \ddots \\ 0 & 0 & \cdots \\ \beta_{lk} & 0 & \cdots \end{pmatrix}. \quad (3.5)$$

Giving dimensions of  $1 \times N_L$  for  $\hat{V}_{dL} = \hat{V}_{Ld}^\dagger$ ,  $N_{L(K)} \times N_{L(K)}$  for  $\hat{H}_{L(K)}$ , and  $N_L \times N_K$  for  $\hat{V}_{LK} = \hat{V}_{KL}^\dagger$ . In order to impose the DLvN boundary conditions on the eigenstates of the driven lead the following unitary ‘‘site-to-state’’ transformation is performed (see Fig. 3) [42]:

$$\hat{U} = \begin{pmatrix} 1 & \hat{0} & \hat{0} \\ \hat{0} & \hat{U}_L & \hat{0} \\ \hat{0} & \hat{0} & \hat{U}_K \end{pmatrix}, \quad (3.6)$$

where  $\hat{U}_L$  and  $\hat{U}_K$  are the unitary matrices that diagonalize  $\hat{H}_L$  and  $\hat{H}_K$ , respectively, such that  $\hat{H}_{L/K} = \hat{U}_{L/K}^\dagger \hat{H}_{L/K} \hat{U}_{L/K} = \text{diag} \{ \varepsilon_{L/K} \}$ . The transformed Hamiltonian matrix has the same block structure as its real-space counterpart:

$$\hat{H}(t) = \hat{U}^\dagger \hat{H}(t) \hat{U} = \begin{pmatrix} \varepsilon_d(t) & \tilde{V}_{dL} & \hat{0} \\ \tilde{V}_{Ld} & \tilde{H}_L & \tilde{V}_{LK} \\ \hat{0} & \tilde{V}_{KL} & \tilde{H}_K \end{pmatrix}, \quad (3.7)$$

where  $\tilde{V}_{dL} = \hat{V}_{Ld}^\dagger$  hold the couplings between the dot and the various lead levels and  $\tilde{V}_{LK} = \hat{V}_{KL}^\dagger$  store the couplings between the latter and the different driven lead levels (see right panel of Fig. 3). In order to mimic the simulation conditions used above, where the dot is uniformly coupled to all lead levels, we replace all elements in  $\tilde{V}_{dL}$  (and  $\tilde{V}_{Ld}^\dagger$ ) by their highest value of  $V \simeq 0.0158$  eV constituting the maximum of the corresponding Newns Anderson coupling band [43]. Given the density of lead states,  $\rho = 50 / (4\beta_l) = 62.5$  eV<sup>-1</sup>, this yields  $\hbar\gamma = 0.0985$  eV (see Eq. 2.4 above), which is comparable to the value of 0.1 eV used above.

The resulting DLvN equation of motion, written in the basis of eigenstates of the dot, lead, and driven lead sections, has the form:

$$\frac{d}{dt} \hat{\sigma}(t) = -\frac{i}{\hbar} [\hat{H}(t), \hat{\sigma}(t)] - \Gamma \cdot \begin{pmatrix} 0 & \hat{0} & \frac{1}{2} \hat{\sigma}_{dK}(t) \\ \hat{0} & \hat{0} & \frac{1}{2} \hat{\sigma}_{LK}(t) \\ \frac{1}{2} \hat{\sigma}_{Kd}(t) & \frac{1}{2} \hat{\sigma}_{KL}(t) & \hat{\sigma}_K(t) - \hat{\sigma}_K^0 \end{pmatrix}, \quad (3.8)$$

where  $\hat{\sigma}_K^0$  is the target equilibrium density matrix imposed by the implicit bath on the driven-lead section with  $\mu = 0$  and  $k_B T = 0.25 \hbar\gamma$  and the driving rate is chosen as  $\Gamma = 2 / (\hbar\rho) = 0.0486$  fs<sup>-1</sup>. When setting  $d\hat{\sigma}/dt = 0$  (see Appendix B), the energy resolved currents between the dot and the lead section now vanish (see dashed black curve in Fig. 2) as required. Nevertheless, the equilibrium state of the entire finite system remains approximate and the spurious currents have been just driven away toward the (less physically relevant) interface between the lead and the driven lead sections. This is demonstrated by the dashed green curve in Fig. 2, where we plot the total current flowing from the lead section to the various driven lead levels,  $k$ , calculated via

$$J_{LK}(\varepsilon_k) = \frac{2}{\hbar} \sum_l^{N_L} (\Im(H_{kl} \sigma_{lk}(t))). \quad (3.9)$$

This, therefore, clearly demonstrates that care should be exercised when utilizing numerical schemes using finite models to simulate (thermo)dynamic properties of open quantum systems. Brute force application of such schemes may lead to unphysical results that are strongly influenced by the applied boundary conditions.

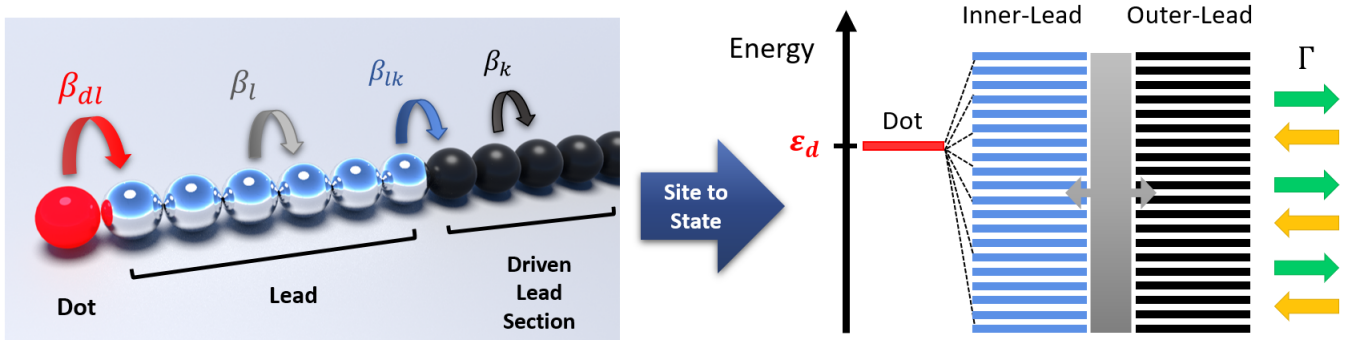


Figure 3: Site-to-state transformation. Left: Schematic site representation of the tight-binding model for a one dimensional chain composed of a dot (red), a lead (silver), and a driven-lead section (black).  $\beta_l$  and  $\beta_k$  denote the hopping integrals within the lead and the driven-lead sections, respectively.  $\beta_{dl}$  and  $\beta_{lk}$  are the coupling matrix elements between the dot and the leftmost site of the lead and between the rightmost site of the lead and the leftmost site of the driven-lead section, respectively. Right: Scheme of the single-particle state representation, where the dot level is uniformly coupled to the eigenstates of the lead section that are separately coupled to the manifold of eigenstates of the driven-lead section that, in turn, are equilibrated at a rate  $\Gamma$  with the implicit external bath.

## 4 Finite Bandwidth Effects

The numerical examples provided above considered a static dot level placed sufficiently far from the lead's band-edges and situated symmetrically between them. In non-equilibrium thermodynamic calculations, however, we will often be interested in simulating time-dependent perturbations applied to the system. These may include time-dependent external fields or varying gate potentials that dynamically shift the dot's level energy. In such cases, it may become inevitable to position the dot level in the vicinity of the lead's band edges. Hence, it is important to understand both the physical and the numerical implications of approaching the band-edges of the modeled environment. This is especially true in the context of comparisons with, and extensions of, analytical treatments that, as stated above, often make simplifying assumptions, such as the WBA (see Sec. 3 above) that treats the environment as an infinite energy band of uniform and continuous density-of-states.

To demonstrate this, we study the changes in equilibrium total number of particles and electronic energy of the finite system upon shifting the dot away from the band center towards the upper band edge. Comparing the results for increasing band-widths to the predictions of the analytical WBA treatment allows us to assess the importance of band-edge effects and the convergence of the numerical model to the WBL. To this end, we consider the isolated system consisting of the dot level and a finite lead manifold of  $N_l$  states. We choose a uniform density of lead levels of  $\rho = 10(\hbar\gamma)^{-1}$  that are uniformly coupled to the dot level via  $V = \sqrt{\frac{\hbar\gamma}{2\pi\rho}} = \frac{\hbar\gamma}{\sqrt{20\pi}}$  (see Eq. 2.3). The dot level is first positioned at the center of the lead levels band,  $\epsilon_d = 0$ , and the Hamiltonian

matrix of the entire closed system is diagonalized. The eigenstates are then occupied according to the Fermi-Dirac distribution and the equilibrium number of particles and total electronic energy are calculated as:

$$N(\varepsilon_d = 0, W) = \sum_{j=0}^{N_l+1} f_{FD}(\varepsilon_j; \mu = 0, T = 0.25\hbar\gamma/k_B) \quad (4.1)$$

and

$$E(\varepsilon_d = 0, W) = \sum_{j=0}^{N_l+1} f_{FD}(\varepsilon_j; \mu = 0, T = 0.25\hbar\gamma/k_B) \varepsilon_j, \quad (4.2)$$

respectively, where  $W = N_l/\rho$ . Similarly, we obtain  $N(\varepsilon_d = 2\hbar\gamma, W)$  and  $E(\varepsilon_d = 2\hbar\gamma, W)$  by positioning the dot level  $2\hbar\gamma$  above the lead's band center, and calculate the variations  $\Delta N_{num}(W) = N(\varepsilon_d = 2\hbar\gamma, W) - N(\varepsilon_d = 0, W)$  and  $\Delta E_{num}(W) = E(\varepsilon_d = 2\hbar\gamma, W) - E(\varepsilon_d = 0, W)$ . To assess the correspondence between the numerical calculation and the analytical WBA results we repeat this procedure for increasing lead's bandwidth by increasing the number of lead states while keeping their density fixed. At the limit of infinite bandwidth we expect the numerical results to converge to the analytical WBA values of:

$$\Delta N_{analytic} = \int_{-\infty}^{\infty} [A(\varepsilon - 2\hbar\gamma; \Delta = 0; \gamma) - A(\varepsilon - 0; \Delta = 0; \gamma)] f_{FD}(\varepsilon; \mu = 0, T = 0.25\hbar\gamma/k_B) d\varepsilon \quad (4.3)$$

and

$$\Delta E_{analytic} = \int_{-\infty}^{\infty} [A(\varepsilon - 2\hbar\gamma; \Delta = 0; \gamma) - A(\varepsilon - 0; \Delta = 0; \gamma)] f_{FD}(\varepsilon; \mu = 0, T = 0.25\hbar\gamma/k_B) \varepsilon d\varepsilon. \quad (4.4)$$

In practice, we calculate these integrals numerically with integration bounds of  $W = 3000\hbar\gamma$ , such that increasing the bounds to  $W = 3500\hbar\gamma$  gives a difference of 0.02% for the energy and  $9 \times 10^{-6}\%$  for the particle number. Note that when comparing the numerical results to the analytical values, the lead levels occupations are assumed to be insensitive to the dot level position such that  $\Delta N_{num}$  and  $\Delta E_{num}$  reflect only the change in dot occupation and energy contribution, like their analytical counterparts. Fig. 4 shows the relative deviation of the change of number of particles (full blue line) with respect to the analytical WBA result  $\Delta\Delta N(W) = [\Delta N_{num}(W) - \Delta N_{analytic}]/\Delta N_{analytic}$  and the corresponding relative energy deviation (full red line)  $\Delta\Delta E(W) = [\Delta E_{num}(W) - \Delta E_{analytic}]/\Delta E_{analytic}$  as a function of bandwidth,  $W$ . We find that, for a finite band model, the change in number of particles upon the upshift of the dot level from the band center is larger than the analytical WBA result, whereas the corresponding change in electronic energy is smaller than its WBA counterpart. As expected, both  $\Delta N_{num}$  and  $\Delta E_{num}$  converge to the corresponding analytical WBL values with increasing finite lead model bandwidth. Notably, the particle number change converges faster than the electronic energy

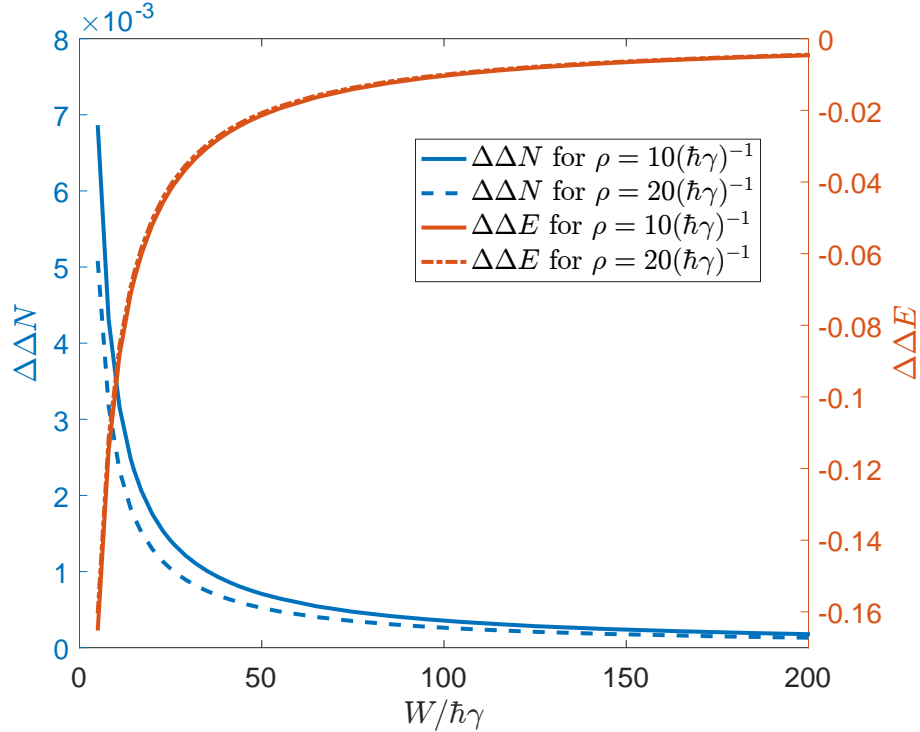


Figure 4: Convergence of the calculated equilibrium occupation,  $\Delta\Delta N$  (blue), and electronic energy,  $\Delta\Delta E$  (red), variations of the finite lead model system towards the wide band limit. The results are obtained for lead density of lead states of  $\rho = 10(\hbar\gamma)^{-1}$  (full lines) and  $\rho = 20(\hbar\gamma)^{-1}$  (dashed lines).

change, such that at a bandwidth of  $200\hbar\gamma$  the deviation of  $\Delta N_{num}$  from  $\Delta N_{analytic}$  reduces to 0.02% while the corresponding deviation in the electronic energy is still larger than 0.5%. To rationalize this observation we note that the integrand of  $\Delta E_{analytic}$  includes  $\varepsilon$  itself, which diverges at the integration limits, and hence slows the convergence of the integrand at any finite integration range. This exemplifies a general behavior that different observables converge at a different rate with system parameters, thus care should be taken to separately converge them. To further verify that these results are converged with respect to the choice of density of lead levels we have repeated the calculations for a density of  $\rho = 20(\hbar\gamma)^{-1}$  obtaining only minor deviations for the particle number and energy variations (see dashed blue and red lines in Fig. 4). The analysis presented above thus demonstrates that numerical treatments can simulate various environment models ranging from simplistic wide-band baths to more complex finite-band baths that are not restricted to uniform density-of-states and/or system bath couplings.

The same holds true not only for simulating complex bath models but also for studying dynamical processes of the system itself. In the resonant level model discussed herein the latter may translate to dynamical shifts of the dot's level energy across the lead's band. Nevertheless, prior to performing dynamical simulations one should first verify that the numerical approach can reproduce quasi-static results. To this end, we repeated the procedure detailed above using a finite

lead model consisting of 500 levels spanning a bandwidth of  $W = 10\hbar\gamma$ , which, according to Fig. 4, reproduces WBA occupations and energetics down to  $\sim 0.4\%$  and  $\sim 9.5\%$ , respectively. The dot level is then uniformly coupled to all lead states with  $V = \frac{\hbar\gamma}{\sqrt{100\pi}}$  and its energy is varied around the chemical potential of the lead. For each dot level position,  $\varepsilon_d$ , the Hamiltonian of the entire finite model system is diagonalized and its eigenstates,  $\{|j\rangle\}$ , are occupied according to the equilibrium Fermi-Dirac distribution. As our observable we choose the dot section contribution to the total electronic energy of the system. In the above treatment we have assumed that the lead section populations are insensitive to the dot level position, such that any change in total energy of the system reflects only the dot's contribution. Alternatively, we can evaluate it in the eigenbasis of the entire system via  $E_d^{num}(\varepsilon_d) = \sum_j \varepsilon_j f(\varepsilon_j) |\langle d|j\rangle|^2$ , where the sum runs over all eigenstates, and their individual contributions to the total electronic energy  $\varepsilon_j f(\varepsilon_j)$  ( $\varepsilon_j$  and  $f(\varepsilon_j)$  being the orbital energy and equilibrium occupation, respectively) are scaled by their projection on the dot section,  $|\langle d|j\rangle|^2$ . In Fig. 5 we compare the numerical value (full blue line) obtained for  $\Delta E_d^{num}(\varepsilon_d) = E_d^{num}(\varepsilon_d) - E_d^{num}(\mu = 0)$  at various dot level positions in a range of  $\pm 2\hbar\gamma$  around the chemical potential (which is kept fix at  $\mu = 0$ ) and an electronic temperature of  $T = 0.25\hbar\gamma/k_B$ , to the analytical WBA results (dashed black line) obtained, as above, from:

$$\Delta E_d^{analytic}(\varepsilon_d) = \int_{-\infty}^{\infty} [A(\varepsilon - \varepsilon_d; \Delta = 0; \gamma) - A(\varepsilon - \mu; \Delta = 0; \gamma)] f_{FD}(\varepsilon; \mu = 0, T = 0.25\hbar\gamma/k_B) \varepsilon d\varepsilon. \quad (4.5)$$

As noted above, in practice we calculate these integrals numerically with integration bounds of  $W = 3000\hbar\gamma$ . In the vicinity of the lead's Fermi energy the agreement between the two calculations is seen to be excellent. Minor deviations between the two develop as the dot position approaches the band edges of the finite lead model (see inset of Fig. 5). To avoid such finite-bandwidth effects and achieve better agreement between the numerical results and the analytical wide band approximation we suggest an alternative approach, where the dot level is kept fixed at the lead's band center (symmetrically between the two band edges) and the chemical potential of the lead is varied around it. The results of this practice are presented by the full red line in Fig. 5 showing better agreement with the analytical WBA results as is clearly demonstrated in the inset.



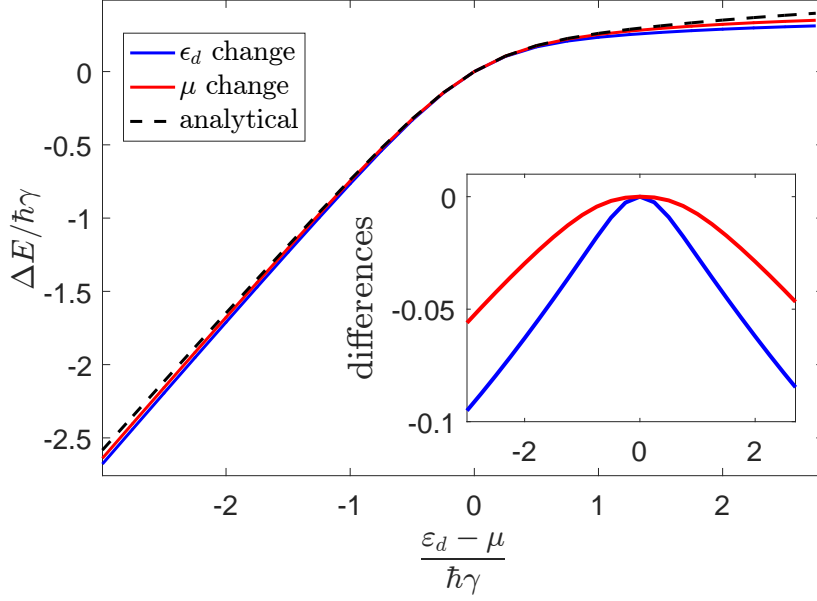


Figure 5: Comparison between the numerical evaluation (full blue and red lines) of the contribution to the total equilibrium electronic energy of a dot that is uniformly coupled to a discrete set of lead levels of finite bandwidth and the corresponding analytical WBA result (dashed black line). The numerical evaluation is performed either by shifting the dot’s position while keeping the chemical potential fixed at the lead band center (blue) or vice versa (red). In all graphs, the Y-axis origin is set to the dot’s contribution to the total energy when placed, along with the chemical potential, at the center of the lead’s band. **Inset:** The differences between the numerical and the analytical evaluations of the dot’s energy contribution to the total equilibrium electronic energy as a function of its position along the leads band. The line colors correspond to those in the main panel.

Having established that our method can reproduce quasi-static results we can now turn to discuss dynamic variations of the dot’s level position. Simulating such processes with the closed system treatment presented above will require extremely large lead models to prevent backscattering from the finite-model boundaries during the relevant simulation time-scales. As demonstrated above, this can be readily avoided by using the DLvN approach, where broadening of the discrete manifold of levels of a relatively small finite lead model allows to mimic the continuous density-of-state of a (semi-)infinite bath. Result of such simulations can provide valuable dynamical information for finite band bath models. However, one might also wish to use the numerical treatment to study dynamical processes in the wide bath band limit, which cannot be accessed using current analytical treatments. Here, as well, we could increase the finite lead model until convergence with respect to its bandwidth is obtained. Within the context of dynamical simulations, however, this would considerably increase the computational burden and defeat the main purpose of the DLvN approach. Hence, again, we offer an alternative by assuming that the difference between the numerical finite-lead-band result and the analytical WBA results depend weakly on the rate

of dot level shift. If this assumption is valid, we can extract this difference from a quasi-static calculation, where both numerical and analytical results are available:

$$\delta E_d(\varepsilon_d) = E_d^{num, QS}(\varepsilon_d) - E_d^{analytic, QS}(\varepsilon_d). \quad (4.6)$$

By subtracting this difference from the dynamic finite-bandwidth model numerical results we obtain an estimate of the corresponding WBL results. To demonstrate this, we use a relatively small lead model consisting of  $N_L = 100$  lead states spanning a bandwidth of  $W = 10\hbar\gamma$ . Notably, the latter is taken deliberately insufficient to achieve convergence to the WBL (see Fig. 4). We solve the DLvN equation of motion using a driving rate of  $\Gamma = 0.2\hbar\gamma$ , and a target density that provides a chemical potential of  $\mu = 0$  and an electronic temperature of  $k_B T = 0.25\gamma$ , starting at equilibrium with the dot level positioned at  $\varepsilon_d = \mu - 3\hbar\gamma$  and shifting it at a constant rate of  $\dot{\varepsilon}_d/(\hbar\gamma^2) = 0.6582$  up to  $\varepsilon_d = \mu + 3\hbar\gamma$ . Using the density matrix of the entire system we can evaluate the temporal evolution of the dot's contribution to the total electronic energy using the following projection:

$$E_d^{num}(t) = \frac{1}{2} \langle d | \hat{H}(t) \hat{\sigma}(t) + \hat{\sigma}(t) \hat{H}(t) | d \rangle, \quad (4.7)$$

which is symmetrized to be real valued.

The results of this calculation (full blue line in Fig. 6) differ from the quasi-static analytical WBA results (full red line in Fig. 6) over the entire range of dot positions studied. This can be attributed to two main factors: (i) the finite lead bandwidth of the numerical model compared to the infinite bath band assumed in the analytical case; and (ii) the finite dot level shift rate used in the numerical simulation, which pushes the system out of its equilibrium state that is assumed by the quasi-static analytical treatment. Under the assumption mentioned above, we can eliminate the effect of the former by adding  $\delta E_d(\varepsilon_d(t)) = \delta E_d(\mu - 3\hbar\gamma + \dot{\varepsilon}_d t)$  to the calculated  $E_d^{num}(t)$ . This allows us to estimate effects of dynamical dot level shifts at the wide-band bath limit. Comparing the red line in Fig. 6 for  $E_d^{num, WBA}(t) = E_d^{num}(t) - \delta E_d(\varepsilon_d(t))$  to the dashed black line for  $E_d^{analytic, QS}(\varepsilon_d)$  we see that, up to the lead's Fermi energy the dynamical result resemble the quasi-static behavior, exhibiting a linear increase. This reflects the fact that in this region the dot remains fully occupied and the variation of the dot's contribution to the total electronic energy stems only from changing its position. When approaching the Fermi level, the dot gradually empties into the lead. Hence the energy rise of  $E_d^{num, WBA}(t)$  due to the upshift of  $\varepsilon_d$  is countered by the dot's depopulation and its slope reduces. Noticeably, when the rate of the dot level up-shift becomes comparable or larger than  $\gamma$ , its emptying into the lead lags behind that of the quasi-static case. This results in the rate-dependent hysteresis evident in Fig. 6, where  $E_d^{num, WBA}(t)$  overshoots  $E_d^{analytic, QS}(\varepsilon_d)$  in the vicinity of the lead Fermi energy. The analysis presented above thus demonstrates how DLvN based simulations can be used to study dynamical effects in open quantum systems in a wide range of system and bath parameters and extract important information relevant for evaluating their non-equilibrium thermodynamic properties.

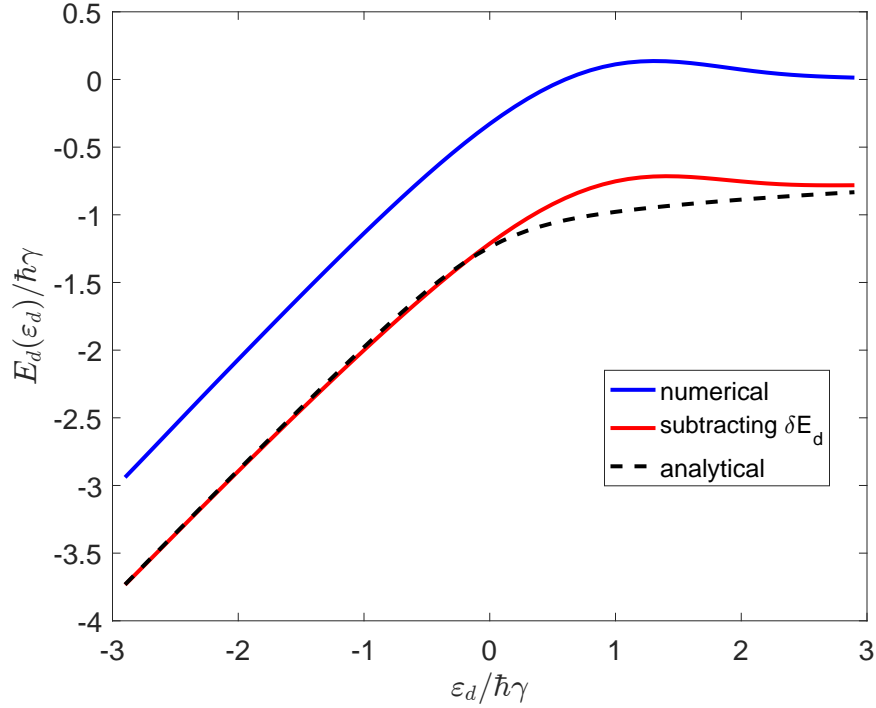


Figure 6: Dynamic contribution (full blue line) to the total electronic energy due to a dot that is up-shifted at a finite rate across a discrete set of lead levels of finite bandwidth, to which it is uniformly coupled. Estimation of the corresponding WBL behavior, obtained by subtracting  $\delta E_d(\varepsilon_d(t))$  from the simulation results, is presented in red. The quasi-static analytical WBA results are given as reference by the dashed black line.

## 5 Summary and Conclusions

The study of non-equilibrium dynamics and thermodynamics of open quantum systems is currently gaining increasing theoretical and experimental interest. Simple analytical treatments provide valuable insights regarding the extension of thermodynamic quantities towards non-equilibrium conditions. These, however, are often based on simplifying assumptions regarding the structure of the system, the environment, and their inter-coupling, thus limiting their validity to specific parameter ranges. Numerical approaches, such as the Driven Liouville-von Neumann methodology, can help bridge the gap between phenomenological analytical treatments and realistic experimental scenarios. In this paper, we presented a brief outline of the DLvN approach and discussed some important methodological aspects of its utilization for studying non-equilibrium (thermo)dynamic properties. Specifically, we have demonstrated that DLvN simulations using finite model systems can capture the depopulation dynamics of an impurity electronic state uniformly coupled to an infinite bath of continuous and constant density of states. We have shown that when evaluating energy resolved quantities based on DLvN simulations, care should be taken to avoid the effects of spurious equilibrium currents resulting from the inherently approximate equilibrium state imposed on the system. We have further studied the convergence of DLvN numerical simulations towards the wide band bath limit upon increase in the bandwidth of the finite lead model. Finally, we have shown how one can obtain reliable static and dynamic wide band results using relatively small model systems either via efficient cancellation of finite-bandwidth effect or by their direct subtraction from the simulated properties. Importantly, these methodological considerations may be relevant to other numerical techniques for simulating electron dynamics in open quantum systems. Hence, with the understanding gained herein, numerical approaches, such as the DLvN methodology, may become efficient tools for simulating non-equilibrium quantum thermodynamics in experimentally relevant regimes that are out of the reach of current analytical treatments.

## 6 Acknowledgments

IO gratefully acknowledges the support of the Adams Fellowship Program of the Israel Academy of Sciences and Humanities, and the Naomi Foundation through the Tel-Aviv University GRTF Program. The research of AN is supported by the U.S. National Science Foundation (Grant No. CHE1665291), the Israel-U.S. Binational Science Foundation, the German Research Foundation (DFG *TH* 820/11-1), and the University of Pennsylvania. OH is grateful for the generous financial support of the Israel Science Foundation under Grant No. 1740/13 and the Center for Nanoscience and Nanotechnology of Tel-Aviv University.

## References

- [1] Abraham Nitzan and Mark A. Ratner. Electron Transport in Molecular Wire Junctions. *Science*, 300(5624):1384–1389, 2003.
- [2] Juan Carlos Cuevas and Elke Scheer. *Molecular Electronics: An Introduction to Theory and Experiment*. World Scientific series in nanoscience and nanotechnology ; v. 1. World Scientific, 2010.
- [3] Avik Ghosh. *Nanoelectronics A Molecular View*. World Scientific, 2016.
- [4] Michael Galperin and Abraham Nitzan. Molecular optoelectronics: the interaction of molecular conduction junctions with light. *Physical Chemistry Chemical Physics*, 14(26):9421, 2012.
- [5] Anton Bruch, Mark Thomas, Silvia Viola Kusminskiy, Felix von Oppen, and Abraham Nitzan. Quantum thermodynamics of the driven resonant level model. *Physical Review B*, 93(11):115318, March 2016.
- [6] María Florencia Ludovico, Jong Soo Lim, Michael Moskalets, Liliana Arrachea, and David Sánchez. Dynamical energy transfer in ac-driven quantum systems. *Physical Review B*, 89(16):161306(R), April 2014.
- [7] María Florencia Ludovico, Michael Moskalets, David Sánchez, and Liliana Arrachea. Dynamics of energy transport and entropy production in ac-driven quantum electron systems. *Physical Review B*, 94(3):035436, July 2016.
- [8] Massimiliano Esposito, Maicol A. Ochoa, and Michael Galperin. Quantum Thermodynamics: A Nonequilibrium Green’s Function Approach. *Physical Review Letters*, 114(8):080602, February 2015.
- [9] Riku Tuovinen, Niko Säkkinen, Daniel Karlsson, Gianluca Stefanucci, and Robert van Leeuwen. Phononic heat transport in the transient regime: An analytic solution. *Physical Review B*, 93(21):214301, June 2016.
- [10] David Gelbwaser-Klimovsky, Wolfgang Niedenzu, and Gershon Kurizki. Thermodynamics of Quantum Systems Under Dynamical Control. In *Advances In Atomic, Molecular, and Optical Physics*, volume 64, pages 329–407. Elsevier, 2015.
- [11] Liliana Arrachea, Eduardo R. Mucciolo, Claudio Chamon, and Rodrigo B. Capaz. Microscopic model of a phononic refrigerator. *Physical Review B*, 86(12):125424, September 2012.
- [12] Ronnie Kosloff and Amikam Levy. Quantum Heat Engines and Refrigerators: Continuous Devices. *Annual Review of Physical Chemistry*, 65(1):365–393, April 2014.

- [13] Hartmut Haug and Antti-Pekka Jauho. *Quantum Kinetics in Transport and Optics of Semiconductors*, volume 123. Springer-Verlag Berlin Heidelberg, 2 edition, 2008.
- [14] Liping Chen, Thorsten Hansen, and Ignacio Franco. Simple and Accurate Method for Time-Dependent Transport along Nanoscale Junctions. *The Journal of Physical Chemistry C*, 118(34):20009–20017, August 2014.
- [15] Chiao-Lun Cheng, Jeremy S. Evans, and Troy Van Voorhis. Simulating molecular conductance using real-time density functional theory. *Physical Review B*, 74(15):155112, October 2006.
- [16] M Di Ventra and T N Todorov. Transport in nanoscale systems: the microcanonical versus grand-canonical picture. *Journal of Physics: Condensed Matter*, 16(45):8025–8034, November 2004.
- [17] Tamar Seideman and William H. Miller. Calculation of the cumulative reaction probability via a discrete variable representation with absorbing boundary conditions. *The Journal of Chemical Physics*, 96(6):4412–4422, March 1992.
- [18] Roi Baer and Ronnie Kosloff. Quantum dissipative dynamics of adsorbates near metal surfaces: A surrogate Hamiltonian theory applied to hydrogen on nickel. *The Journal of Chemical Physics*, 106(21):8862–8875, June 1997.
- [19] Christiane P. Koch, Thorsten Klüner, Hans-Joachim Freund, and Ronnie Kosloff. Femtosecond Photodesorption of Small Molecules from Surfaces: A Theoretical Investigation from First Principles. *Physical Review Letters*, 90(11):117601, March 2003.
- [20] Michael Galperin and Abraham Nitzan. Current-Induced Light Emission and Light-Induced Current in Molecular-Tunneling Junctions. *Physical Review Letters*, 95(20):206802, November 2005.
- [21] U Kleinekathöfer, GuangQi Li, S Welack, and M Schreiber. Switching the current through model molecular wires with Gaussian laser pulses. *Europhysics Letters (EPL)*, 75(1):139–145, July 2006.
- [22] B. D. Fainberg, M. Jouravlev, and A. Nitzan. Light-induced current in molecular tunneling junctions excited with intense shaped pulses. *Physical Review B*, 76(24):245329, December 2007.
- [23] Gil Katz, David Gelman, Mark A. Ratner, and Ronnie Kosloff. Stochastic surrogate Hamiltonian. *The Journal of Chemical Physics*, 129(3):034108, July 2008.
- [24] Joseph E. Subotnik, Thorsten Hansen, Mark A. Ratner, and Abraham Nitzan. Nonequilibrium steady state transport via the reduced density matrix operator. *The Journal of Chemical Physics*, 130(14):144105, April 2009.

- [25] Adam E. Rothman and David A. Mazziotti. Nonequilibrium, steady-state electron transport with N-representable density matrices from the anti-Hermitian contracted Schrödinger equation. *The Journal of Chemical Physics*, 132(10):104112, March 2010.
- [26] Roie Volkovich and Uri Peskin. Transient dynamics in molecular junctions: Coherent bichromophoric molecular electron pumps. *Physical Review B*, 83(3):033403, January 2011.
- [27] N. Renaud, M. A. Ratner, and C. Joachim. A Time-Dependent Approach to Electronic Transmission in Model Molecular Junctions, February 2011.
- [28] Uri Peskin and Michael Galperin. Coherently controlled molecular junctions. *The Journal of Chemical Physics*, 136(4):044107, January 2012.
- [29] Triet S. Nguyen, Ravindra Nanguneri, and John Parkhill. How electronic dynamics with Pauli exclusion produces Fermi-Dirac statistics. *The Journal of Chemical Physics*, 142(13):134113, April 2015.
- [30] Roi Baer and Daniel Neuhauser. Ab initio electrical conductance of a molecular wire. *International Journal of Quantum Chemistry*, 91(3):524–532, 2003.
- [31] Roi Baer, Tamar Seideman, Shahal Ilani, and Daniel Neuhauser. Ab initio study of the alternating current impedance of a molecular junction. *The Journal of Chemical Physics*, 120(7):3387–3396, February 2004.
- [32] Neil Bushong, Na Sai, and Massimiliano Di Ventra. Approach to Steady-State Transport in Nanoscale Conductors. *Nano Letters*, 5(12):2569–2572, December 2005.
- [33] Cristián G. Sánchez, Maria Stamenova, Stefano Sanvito, D. R. Bowler, Andrew P. Horsfield, and Tchavdar N. Todorov. Molecular conduction: Do time-dependent simulations tell you more than the Landauer approach? *The Journal of Chemical Physics*, 124(21):214708, June 2006.
- [34] Xiao Zheng, Fan Wang, Chi Yung Yam, Yan Mo, and GuanHua Chen. Time-dependent density-functional theory for open systems. *Physical Review B*, 75(19):195127, May 2007.
- [35] Jeremy S. Evans and Troy Van Voorhis. Dynamic Current Suppression and Gate Voltage Response in Metal-Molecule-Metal Junctions. *Nano Letters*, 9(7):2671–2675, July 2009.
- [36] İlke Ercan and Neal G. Anderson. Tight-binding implementation of the microcanonical approach to transport in nanoscale conductors: Generalization and analysis. *Journal of Applied Physics*, 107(12):124318, June 2010.
- [37] Xiao Zheng, GuanHua Chen, Yan Mo, SiuKong Koo, Heng Tian, ChiYung Yam, and YiJing Yan. Time-dependent density functional theory for quantum transport. *The Journal of Chemical Physics*, 133(11):114101, September 2010.

- [38] Yanxia Xing, Bin Wang, and Jian Wang. First-principles investigation of dynamical properties of molecular devices under a steplike pulse. *Physical Review B*, 82(20):205112, November 2010.
- [39] San-Huang Ke, Rui Liu, Weitao Yang, and Harold U. Baranger. Time-dependent transport through molecular junctions. *The Journal of Chemical Physics*, 132(23):234105, June 2010.
- [40] Rulin Wang, Dong Hou, and Xiao Zheng. Time-dependent density-functional theory for real-time electronic dynamics on material surfaces. *Physical Review B*, 88(20):205126, November 2013.
- [41] Philipp Schaffhauser and Stephan K ummel. Using time-dependent density functional theory in real time for calculating electronic transport. *Physical Review B*, 93(3):035115, January 2016.
- [42] Tamar Zelovich, Leeor Kronik, and Oded Hod. State Representation Approach for Atomistic Time-Dependent Transport Calculations in Molecular Junctions. *Journal of Chemical Theory and Computation*, 10(8):2927–2941, August 2014.
- [43] Tamar Zelovich, Leeor Kronik, and Oded Hod. Molecule-Lead Coupling at Molecular Junctions: Relation between the Real- and State-Space Perspectives. *Journal of Chemical Theory and Computation*, 11(10):4861–4869, October 2015.
- [44] Tamar Zelovich, Leeor Kronik, and Oded Hod. Driven Liouville von Neumann Approach for Time-Dependent Electronic Transport Calculations in a Nonorthogonal Basis-Set Representation. *The Journal of Physical Chemistry C*, 120(28):15052–15062, July 2016.
- [45] Tamar Zelovich, Thorsten Hansen, Zhen-Fei Liu, Jeffrey B. Neaton, Leeor Kronik, and Oded Hod. Parameter-free driven Liouville-von Neumann approach for time-dependent electronic transport simulations in open quantum systems. *The Journal of Chemical Physics*, 146(9):092331, March 2017.
- [46] Oded Hod, Cesar A. Rodriguez-Rosario, Tamar Zelovich, and Thomas Frauenheim. Driven Liouville von Neumann Equation in Lindblad Form. *The Journal of Physical Chemistry A*, 120(19):3278–3285, May 2016.
- [47] Daniel Gruss, Kirill A. Velizhanin, and Michael Zwolak. Landauer’s formula with finite-time relaxation: Kramers’ crossover in electronic transport. *Scientific Reports*, 6(1):24514, July 2016.
- [48] Justin E. Elenewski, Daniel Gruss, and Michael Zwolak. Communication: Master equations for electron transport: The limits of the Markovian limit. *The Journal of Chemical Physics*, 147(15):151101, October 2017.



- [49] C. J. O. Verzijl, J. S. Seldenthuis, and J. M. Thijssen. Applicability of the wide-band limit in DFT-based molecular transport calculations. *The Journal of Chemical Physics*, 138(9):094102, March 2013.
- [50] Ioan Bâldea. Invariance of molecular charge transport upon changes of extended molecule size and several related issues. *Beilstein Journal of Nanotechnology*, 7:418–431, March 2016.
- [51] F. Covito, F. G. Eich, R. Tuovinen, M. A. Sentef, and A. Rubio. Transient Charge and Energy Flow in the Wide-Band Limit. *Journal of Chemical Theory and Computation*, 14(5):2495–2504, May 2018.
- [52] A. Nitzan. *Chemical Dynamics in Condensed Phases: Relaxation, Transfer and Reactions in Condensed Molecular Systems*. Oxford Graduate Texts. OUP Oxford, 2006.
- [53] Max Koentopp, Connie Chang, Kieron Burke, and Roberto Car. Density functional calculations of nanoscale conductance. *Journal of Physics: Condensed Matter*, 20(8):083203, February 2008.
- [54] S. Kurth, G. Stefanucci, C.-O. Almbladh, A. Rubio, and E. K. U. Gross. Time-dependent quantum transport: A practical scheme using density functional theory. *Physical Review B*, 72(3):035308, July 2005.
- [55] Maicol A. Ochoa, Anton Bruch, and Abraham Nitzan. Energy distribution and local fluctuations in strongly coupled open quantum systems: The extended resonant level model. *Physical Review B*, 94(3):035420, July 2016.
- [56] Uriel N. Morzan, Francisco F. Ramírez, Mariano C. González Lebrero, and Damián A. Scherlis. Electron transport in real time from first-principles. *The Journal of Chemical Physics*, 146(4):044110, January 2017.
- [57] Mordechai Bixon and Joshua Jortner. Intramolecular Radiationless Transitions. *The Journal of Chemical Physics*, 48(2):715–726, January 1968.
- [58] Benny Carmeli, Roberto Tulman, Abraham Nitzan, and M. H. Kalos. Random coupling models.IV. Numerical investigation of the dependence on the random coupling distribution and on the initial phases. *Chemical Physics*, 72(3):363 – 369, 1982.

## A Energy Resolved Currents Calculation

Energy resolved currents can be evaluated via the time derivatives of the various lead levels populations. Here, we show how the corresponding expression (Eq. 3.2) is obtained for the resonant level system discussed in the main text. For a system composed of a single dot level and a manifold of lead states that are directly coupled to an implicit bath (Eq. 2.7), the DLvN equation

of motion is given by the following matrix representation written in the basis of eigenstates of the isolated dot and lead sections (Eq. 2.8):

$$\frac{d}{dt} \begin{pmatrix} \sigma_d(t) & \hat{\sigma}_{dL}(t) \\ \hat{\sigma}_{Ld}(t) & \hat{\sigma}_L(t) \end{pmatrix} = -\frac{i}{\hbar} \left[ \begin{pmatrix} \varepsilon_d(t) & \hat{V}_{dL} \\ \hat{V}_{Ld} & \hat{H}_L \end{pmatrix}, \begin{pmatrix} \sigma_d(t) & \hat{\sigma}_{dL}(t) \\ \hat{\sigma}_{Ld}(t) & \hat{\sigma}_L(t) \end{pmatrix} \right] - \Gamma \begin{pmatrix} 0 & \frac{1}{2}\hat{\sigma}_{dL}(t) \\ \frac{1}{2}\hat{\sigma}_{Ld}(t) & \hat{\sigma}_L(t) - \hat{\sigma}_L^0 \end{pmatrix}. \quad (\text{A.1})$$

Evaluating the commutator on the right hand side of Eq. A.1, while taking into consideration that there is a single dot level, gives:

$$\begin{aligned} \frac{d}{dt} \begin{pmatrix} \sigma_d(t) & \hat{\sigma}_{dL}(t) \\ \hat{\sigma}_{Ld}(t) & \hat{\sigma}_L(t) \end{pmatrix} &= -\Gamma \begin{pmatrix} 0 & \frac{1}{2}\hat{\sigma}_{dL}(t) \\ \frac{1}{2}\hat{\sigma}_{Ld}(t) & \hat{\sigma}_L(t) - \hat{\sigma}_L^0 \end{pmatrix} \\ &- \frac{i}{\hbar} \begin{pmatrix} \hat{V}_{dL}\hat{\sigma}_{Ld}(t) - \hat{\sigma}_{dL}(t)\hat{V}_{Ld} & \varepsilon_d(t)\hat{\sigma}_{dL}(t) + \hat{V}_{dL}\hat{\sigma}_L(t) - \sigma_d(t)\hat{V}_{dL} - \hat{\sigma}_{dL}(t)\hat{H}_L \\ \hat{V}_{Ld}\sigma_d(t) + \hat{H}_L\hat{\sigma}_{Ld}(t) - \hat{\sigma}_{Ld}(t)\varepsilon_d(t) - \hat{\sigma}_L(t)\hat{V}_{Ld} & \hat{V}_{Ld}\hat{\sigma}_{dL}(t) + \hat{H}_L\hat{\sigma}_L(t) - \hat{\sigma}_{Ld}(t)\hat{V}_{dL} - \hat{\sigma}_L(t)\hat{H}_L \end{pmatrix}. \end{aligned} \quad (\text{A.2})$$

Hence, the dynamics of the lead section is given by:

$$\frac{d}{dt}\hat{\sigma}_L(t) = -\frac{i}{\hbar} [\hat{H}_L, \hat{\sigma}_L(t)] - \frac{i}{\hbar} [\hat{V}_{Ld}\hat{\sigma}_{dL}(t) - \hat{\sigma}_{Ld}(t)\hat{V}_{dL}] - \Gamma (\hat{\sigma}_L(t) - \hat{\sigma}_L^0). \quad (\text{A.3})$$

From this we can calculate the rate of population variation in a given lead level  $l$  as:

$$\frac{d}{dt}\sigma_{ll}(t) = -\frac{i}{\hbar} \sum_{l'=0}^{N_l} [H_{ll'}\sigma_{l'l}(t) - \sigma_{ll'}(t)H_{l'l}] - \frac{i}{\hbar} [V_{ld}\sigma_{dl}(t) - \sigma_{ld}(t)V_{dl}] - \Gamma (\sigma_{ll}(t) - \sigma_{ll}^0). \quad (\text{A.4})$$

In the representation of the eigenbasis of the isolated dot and lead states,  $\hat{H}_L$  is diagonal and thus the first term on the right hand side of Eq. A.4 vanishes. The remaining two terms can be identified as the particle current flowing between lead state  $l$  and the dot or the implicit bath, respectively. Focusing on the second term and taking into account the fact that  $\hat{H}$  and  $\hat{\sigma}$  are Hermitian matrices, such that  $V_{dl} = V_{ld}^*$  and  $\sigma_{ld}(t) = \sigma_{dl}^*(t)$ , we arrive at the expression for the current flowing between from dot to lead level  $l$  (Eq. 3.2 in the main text):

$$J_{dL}(\varepsilon_l, t) = -\frac{i}{\hbar} [V_{ld}\sigma_{dl}(t) - \sigma_{dl}^*(t)V_{ld}^*] = \frac{2}{\hbar} \Im(V_{ld}\sigma_{dl}(t)). \quad (\text{A.5})$$

If we neglect the lead level width due to its coupling to the bath and the dot,  $J_{dL}(\varepsilon_l, t)$  represents the energy resolved current flowing from the dot to the lead at energy  $\varepsilon_l$ . Correspondingly, the particle current flowing at energy  $\varepsilon_l$  from the lead to the implicit bath is given by (Eq. 3.3 in the main text):

$$J_{LB}(\varepsilon_l, t) = \Gamma (\sigma_{ll}(t) - \sigma_{ll}^0). \quad (\text{A.6})$$

The same holds true when the model system is decomposed into the dot, lead, and driven lead sections (Eq. 3.4 in the main text), where Eq. A.5 remains valid for the current flowing between the dot and lead level  $l$ , and a similar expression is obtained for the current flowing from the lead into driven lead level  $k$ :

$$J_{LK}(\varepsilon_k, t) = \frac{2}{\hbar} \sum_{l=0}^{N_l} \Im (V_{kl} \sigma_{lk}(t)). \quad (\text{A.7})$$

## B Sylvester Equation For the Equilibrium Density Matrix

Within the DLvN approach, the equilibrium state of a single lead setup and the steady-state of a multi-lead setup can be obtained by setting  $\frac{d\hat{\sigma}(t)}{dt} = 0$ . As mentioned in the main text, for the former the obtained equilibrium is approximate as the equation of motion drives only the lead section, rather than the entire system (dot+lead) towards equilibrium. In principle, equilibrium can be reached by running the dynamics until all transient effects relax. This, however, may prove to be computationally quite inefficient, especially when the initial conditions are far from equilibrium. An alternative can be to formulate an equation that directly solves for  $\frac{d\hat{\sigma}(t)}{dt} = 0$  [24]. To this end, in the case of a single lead setup, we define projection operators on the dot and on the lead section as

$$\hat{P} = \begin{pmatrix} 1 & \hat{0} \\ \hat{0} & \hat{0} \end{pmatrix}, \quad \hat{Q} = \begin{pmatrix} 0 & \hat{0} \\ \hat{0} & \hat{1} \end{pmatrix}, \quad (\text{B.1})$$

corresponding to the matrix representation in the basis of the isolated dot and lead eigenfunctions. With these, the driving term in Eq. 2.8 of the main text can be decomposed as follows:

$$\begin{aligned} -\Gamma \cdot \begin{pmatrix} 0 & \frac{1}{2}\hat{\sigma}_{d,L}(t) \\ \frac{1}{2}\hat{\sigma}_{L,d}(t) & \hat{\sigma}_L(t) - \hat{\sigma}_L^0 \end{pmatrix} &= -\frac{1}{2}\Gamma \cdot \underbrace{\begin{pmatrix} 0 & \hat{\sigma}_{d,L}(t) \\ \hat{0} & \hat{0} \end{pmatrix}}_{\hat{P}\hat{\sigma}(t)\hat{Q}} - \frac{1}{2}\Gamma \cdot \underbrace{\begin{pmatrix} 0 & \hat{0} \\ \hat{\sigma}_{L,d}(t) & \hat{0} \end{pmatrix}}_{\hat{Q}\hat{\sigma}(t)\hat{P}} \\ &\quad - \Gamma \cdot \underbrace{\begin{pmatrix} 0 & \hat{0} \\ \hat{0} & \hat{\sigma}_L(t) \end{pmatrix}}_{\hat{Q}\hat{\sigma}(t)\hat{Q}} + \Gamma \cdot \underbrace{\begin{pmatrix} 0 & \hat{0} \\ \hat{0} & \hat{\sigma}_L^0 \end{pmatrix}}_{\hat{Q}\hat{\sigma}^0\hat{Q}}, \end{aligned} \quad (\text{B.2})$$

where in the last term

$$\hat{\sigma}^0 = \begin{pmatrix} \sigma_d^0 & \hat{0} \\ \hat{0} & \hat{\sigma}_L^0 \end{pmatrix}, \quad (\text{B.3})$$

and the target equilibrium occupation of the dot,  $\sigma_d^0$ , does not (and should not) appear in the final expression for the driving term. Nullifying the left hand side of the DLvN equation of motion (Eq. 2.8) with a time-independent Hamiltonian thus gives the following equation for the equilibrium density matrix of the system,  $\hat{\sigma}^{eq}$ :

$$\frac{d}{dt}\hat{\sigma}^{eq} = -\frac{i}{\hbar}\hat{H}\hat{\sigma}^{eq} + \frac{i}{\hbar}\hat{\sigma}^{eq}\hat{H} - \frac{1}{2}\Gamma\hat{P}\hat{\sigma}^{eq}\hat{Q} - \frac{1}{2}\Gamma\hat{Q}\hat{\sigma}^{eq}\hat{P} - \Gamma\hat{Q}\hat{\sigma}^{eq}\hat{Q} + \Gamma\hat{Q}\hat{\sigma}^0\hat{Q} = \hat{0}, \quad (\text{B.4})$$

which can be rearranged as:

$$-\frac{i}{\hbar}\hat{H}\hat{\sigma}^{eq} + \frac{i}{\hbar}\hat{\sigma}^{eq}\hat{H} - \frac{1}{2}\Gamma(\hat{P} + \hat{Q})\hat{\sigma}^{eq}\hat{Q} - \frac{1}{2}\Gamma\hat{Q}\hat{\sigma}^{eq}(\hat{P} + \hat{Q}) + \Gamma\hat{Q}\hat{\sigma}^0\hat{Q} = \hat{0}. \quad (\text{B.5})$$

Since the sum of  $\hat{P}$  and  $\hat{Q}$  gives the unity matrix,  $\hat{1}$ , this results in:

$$\left(\frac{i}{\hbar}\hat{H} + \frac{1}{2}\Gamma\hat{Q}\right)\hat{\sigma}^{eq} - \hat{\sigma}^{eq}\left(\frac{i}{\hbar}\hat{H} - \frac{1}{2}\Gamma\hat{Q}\right) = \Gamma\hat{Q}\hat{\sigma}^0\hat{Q}. \quad (\text{B.6})$$

Defining

$$\hat{A} = \frac{i}{\hbar}\hat{H} + \frac{1}{2}\Gamma\hat{Q} = \frac{i}{\hbar} \begin{pmatrix} \varepsilon_d & \hat{V}_{dL} \\ \hat{V}_{Ld} & \hat{H}_L - \frac{i\hbar}{2}\Gamma\hat{1} \end{pmatrix}, \quad (\text{B.7})$$

$$\hat{B} = \frac{i}{\hbar}\hat{H} - \frac{1}{2}\Gamma\hat{Q} = \frac{i}{\hbar} \begin{pmatrix} \varepsilon_d & \hat{V}_{dL} \\ \hat{V}_{Ld} & \hat{H}_L + \frac{i\hbar}{2}\Gamma\hat{1} \end{pmatrix}, \quad (\text{B.8})$$

and

$$\hat{C} = \Gamma\hat{Q}\hat{\sigma}^0\hat{Q} = \begin{pmatrix} 0 & \hat{0} \\ \hat{0} & \Gamma\hat{\sigma}_L^0 \end{pmatrix}, \quad (\text{B.9})$$

the following Sylvester equation for the equilibrium density matrix is obtained [24]:

$$\hat{A}\hat{\sigma}^{eq} - \hat{\sigma}^{eq}\hat{B} = \hat{C}. \quad (\text{B.10})$$

A similar Sylvester equation can be derived when the system is decomposed into the dot, lead, and driven lead sections. In the basis of eigenfunctions of these isolated sections the corresponding projection operators are written as:

$$\hat{P} = \begin{pmatrix} 1 & \hat{0} & \hat{0} \\ \hat{0} & \hat{0} & \hat{0} \\ \hat{0} & \hat{0} & \hat{0} \end{pmatrix}, \quad \hat{Q} = \begin{pmatrix} 0 & \hat{0} & \hat{0} \\ \hat{0} & \hat{1} & \hat{0} \\ \hat{0} & \hat{0} & \hat{0} \end{pmatrix}, \quad \hat{R} = \begin{pmatrix} 0 & \hat{0} & \hat{0} \\ \hat{0} & \hat{0} & \hat{0} \\ \hat{0} & \hat{0} & \hat{1} \end{pmatrix}. \quad (\text{B.11})$$

The driving term (see Eq. 3.8) can be decomposed in terms of these projection operators as follows:

$$\begin{aligned} & -\Gamma \cdot \begin{pmatrix} 0 & \hat{0} & \frac{1}{2}\hat{\sigma}_{dK}(t) \\ \hat{0} & \hat{0} & \frac{1}{2}\hat{\sigma}_{LK}(t) \\ \frac{1}{2}\hat{\sigma}_{Kd}(t) & \frac{1}{2}\hat{\sigma}_{KL}(t) & \hat{\sigma}_K(t) - \hat{\sigma}_K^0 \end{pmatrix} \\ &= -\frac{1}{2}\Gamma \cdot \underbrace{\begin{pmatrix} 0 & \hat{0} & \hat{0} \\ \hat{0} & \hat{0} & \hat{0} \\ \hat{\sigma}_{Kd}(t) & \hat{0} & \hat{0} \end{pmatrix}}_{\hat{R}\hat{\sigma}(t)\hat{P}} - \frac{1}{2}\Gamma \cdot \underbrace{\begin{pmatrix} 0 & \hat{0} & \hat{0} \\ \hat{0} & \hat{0} & \hat{0} \\ \hat{0} & \hat{\sigma}_{KL}(t) & \hat{0} \end{pmatrix}}_{\hat{R}\hat{\sigma}(t)\hat{Q}} \\ & -\frac{1}{2}\Gamma \cdot \underbrace{\begin{pmatrix} 0 & \hat{0} & \hat{\sigma}_{dK}(t) \\ \hat{0} & \hat{0} & \hat{0} \\ \hat{0} & \hat{0} & \hat{0} \end{pmatrix}}_{\hat{P}\hat{\sigma}(t)\hat{R}} - \frac{1}{2}\Gamma \cdot \underbrace{\begin{pmatrix} 0 & \hat{0} & \hat{0} \\ \hat{0} & \hat{0} & \hat{\sigma}_{LK}(t) \\ \hat{0} & \hat{0} & \hat{0} \end{pmatrix}}_{\hat{Q}\hat{\sigma}(t)\hat{R}} - \Gamma \cdot \underbrace{\begin{pmatrix} 0 & \hat{0} & \hat{0} \\ \hat{0} & \hat{0} & \hat{0} \\ \hat{0} & \hat{0} & \hat{\sigma}_K(t) \end{pmatrix}}_{\hat{R}\hat{\sigma}(t)\hat{R}} + \Gamma \cdot \underbrace{\begin{pmatrix} 0 & \hat{0} & \hat{0} \\ \hat{0} & \hat{0} & \hat{0} \\ \hat{0} & \hat{0} & \hat{\sigma}_K^0 \end{pmatrix}}_{\hat{R}\hat{\sigma}^0\hat{R}}, \end{aligned} \quad (\text{B.12})$$

where, in the last term,

$$\hat{\sigma}^0 = \underbrace{\begin{pmatrix} \sigma_d^0 & \hat{0} & \hat{0} \\ \hat{0} & \sigma_L^0 & \hat{0} \\ \hat{0} & \hat{0} & \sigma_K^0 \end{pmatrix}}, \quad (\text{B.13})$$

and the target equilibrium occupation of the dot ( $\sigma_d^0$ ) and the lead ( $\sigma_L^0$ ) do not (and should not) appear in the final expression for the driving term. Nullifying the left hand side of the DLvN equation of motion (Eq. 3.8) with a time-independent Hamiltonian thus gives the following equation for the equilibrium density matrix of the system,  $\hat{\sigma}^{eq}$ :

$$\frac{d}{dt}\hat{\sigma}^{eq} = -\frac{i}{\hbar}\tilde{H}\hat{\sigma}^{eq} + \frac{i}{\hbar}\hat{\sigma}^{eq}\tilde{H} - \frac{1}{2}\Gamma\hat{R}\hat{\sigma}^{eq}\hat{P} - \frac{1}{2}\Gamma\hat{R}\hat{\sigma}^{eq}\hat{Q} - \frac{1}{2}\Gamma\hat{P}\hat{\sigma}^{eq}\hat{R} - \frac{1}{2}\Gamma\hat{Q}\hat{\sigma}^{eq}\hat{R} - \Gamma\hat{R}\hat{\sigma}^{eq}\hat{R} + \Gamma\hat{R}\hat{\sigma}^0\hat{R} = \hat{0} \quad (\text{B.14})$$

which can be rearranged as:

$$-\frac{i}{\hbar}\tilde{H}\hat{\sigma}^{eq} + \frac{i}{\hbar}\hat{\sigma}^{eq}\tilde{H} - \frac{1}{2}\Gamma\hat{R}\hat{\sigma}^{eq}(\hat{P} + \hat{Q} + \hat{R}) - \frac{1}{2}\Gamma(\hat{P} + \hat{Q} + \hat{R})\hat{\sigma}^{eq}\hat{R} + \Gamma\hat{R}\hat{\sigma}^0\hat{R} = \hat{0}. \quad (\text{B.15})$$

Since the sum of  $\hat{P} + \hat{Q} + \hat{R} = \hat{1}$  this results in:

$$\left(\frac{i}{\hbar}\tilde{H} + \frac{1}{2}\Gamma\hat{R}\right)\hat{\sigma}^{eq} - \hat{\sigma}^{eq}\left(\frac{i}{\hbar}\tilde{H} - \frac{1}{2}\Gamma\hat{R}\right) = \Gamma\hat{R}\hat{\sigma}^0\hat{R}. \quad (\text{B.16})$$

Defining

$$\hat{A} = \frac{i}{\hbar}\tilde{H} + \frac{1}{2}\Gamma\hat{R} = \frac{i}{\hbar} \begin{pmatrix} \varepsilon_d & \tilde{V}_{dL} & \hat{0} \\ \tilde{V}_{Ld} & \tilde{H}_L & \tilde{V}_{LK} \\ \hat{0} & \tilde{V}_{KL} & \tilde{H}_K - \frac{i\hbar}{2}\Gamma\hat{1} \end{pmatrix}, \quad (\text{B.17})$$

$$\hat{B} = \frac{i}{\hbar}\tilde{H} - \frac{1}{2}\Gamma\hat{R} = \frac{i}{\hbar} \begin{pmatrix} \varepsilon_d & \tilde{V}_{dL} & \hat{0} \\ \tilde{V}_{Ld} & \tilde{H}_L & \tilde{V}_{LK} \\ \hat{0} & \tilde{V}_{KL} & \tilde{H}_K + \frac{i\hbar}{2}\Gamma\hat{1} \end{pmatrix}, \quad (\text{B.18})$$

and

$$\hat{C} = \Gamma\hat{R}\hat{\sigma}^0\hat{R} = \begin{pmatrix} 0 & \hat{0} & \hat{0} \\ \hat{0} & \hat{0} & \hat{0} \\ \hat{0} & \hat{0} & \Gamma\hat{\sigma}_K^0 \end{pmatrix}, \quad (\text{B.19})$$

we arrive at a Sylvester equation of the same structure as Eq. B.10 above.